Journal of Alloys and Compounds 642 (2015) 104–110

Contents lists available at ScienceDirect

Journal of Alloys and Compounds

journal homepage: www.elsevier.com/locate/jalcom

Preparation of p-type $AgCrO_2$ nanocrystals through low-temperature hydrothermal method and the potential application in p-type dye-sensitized solar cell

Dehua Xiong [a,b], Huan Wang [a], Wenjun Zhang [a], Xianwei Zeng [a], Haimei Chang [b], Xiujian Zhao [b], Wei Chen [a,*], Yi-Bing Cheng [a,c]

[a] Wuhan National Laboratory for Optoelectronics, Huazhong University of Science and Technology, Wuhan 430074, People's Republic of China
[b] State Key Laboratory of Silicate Materials for Architectures, Wuhan University of Technology, Wuhan 430070, People's Republic of China
[c] Department of Materials Engineering, Monash University, Melbourne, Victoria 3800, Australia

ARTICLE INFO

Article history:
Received 10 February 2015
Received in revised form 9 April 2015
Accepted 11 April 2015
Available online 20 April 2015

Keywords:
Hydrothermal synthesis
p-type semiconductor
Delafossite oxide
Photocathode
Dye-sensitized solar cell

ABSTRACT

The synthesis of nano-sized ternary delafossite oxides with pure crystal phases is of great challenge. We present a novel hydrothermal method for the synthesis of $AgCrO_2$ nanocrystals with ultrafine size of 10–20 nm at relatively low temperature range (190–230 °C). It is the first time to report that $AgCrO_2$ nanocrystals can be hydrothermally synthesized at such a low temperature (190 °C) and applied as photocathode in dye sensitized solar cells (DSSCs). The as-synthesized $AgCrO_2$ nanoproducts, including their crystal phases, morphologies, element compositions, valence state information, thermal stability, electrical and optical properties, have been systematically studied. This facile method employed metal nitrates ($AgNO_3$ and $Cr(NO_3)_3$) as the starting materials and NaOH as the mineralizer, where $Cr(NO_3)_3$ undertook the dual functions of Cr^{3+} source material and weak reducing reagent. The in-situ oxidation–reduction reaction between Cr^{3+} and Ag^+/Cu^{2+} during the hydrothermal crystal growth is the noteworthy feature of this general method. The crystal formation mechanism disclosed in the synthesis of chromium based delafossite oxides will certainly be benefit for the preparation of other delafossite oxides.

1. Introduction

The crystal structure of delafossite oxides, deriving their name from the mineral $CuFeO_2$, was first confirmed by Pabst in 1946 [1]. The delafossite structure is constructed from alternate layers of two-dimensional close-packed copper cations with linear $O–Cu^+–O$ bonds and slightly distorted edge shared $Fe^{3+}O_6$ octahedras [2]. To date, numerous delafossite oxides (AMO_2, A = Ag or Cu, M = B, Al, Ga, In, Fe, Cr, Sc, Y, *etc.*) have been reported to serve important roles in diverse applications, such as photovoltaics, transparent photodiode, catalysts, batteries, ferroelectrics and so on [2,3]. The most attractive features of delafossite oxides should rest with their high p-type conductivity and optical transparency, which have been firstly discovered in $CuAlO_2$ by Hisono et al. and well explained by the "chemical modulation of valance band" theory [4]. Recently, several groups including ours started the applications of delafossite oxides nanocrystalline as the photocathode materials in p-type dye-sensitized solar cells (DSSCs), in replacement of conventional NiO, and several successful examples include $CuAlO_2$ [5,6], $CuGaO_2$ [7–10] and $CuCrO_2$ [11–14]. As reflected in all of the previous works [10–14], size control of the delafossite nanocrystals are critical for the high performance of p-type DSSCs [15,16].

Generally, delafossite oxides powders could be prepared through high temperature solid-state reactions [17–19], cation exchange reactions [19–23], and hydrothermal synthesis [7–14]. However, it is very difficult to synthesize nano-sized crystals of delafossite oxides, which largely restricts their application fields. To the best of our knowledge, only a few literatures focused on the synthesis of nano-sized delafossite oxides; the successful examples are not exceeding $CuAlO_2$ [24], $CuGaO_2$ [7–10,25] and $CuCrO_2$ [11–14,26]. Though, more copper based delafossite oxides ($CuAlO_2$, $CuCrO_2$, $CuFeO_2$, $CuScO_2$ and so on) could be synthesized readily via high temperature solid-state reactions under N_2 or Ar atmosphere at 800–1200 °C [2], avoiding the valence for the monovalent copper (Cu^+) being oxidized into bivalent Cu^{2+}, the higher temperature usually led to excessive growth of big delafossite crystals. Compared with the copper based delafossites, the synthesis of silver based delafossites is even more difficult. The related reports

* Corresponding author. Tel./fax: +86 27 8779 3867.
E-mail address: wnlochenwei@mail.hust.edu.cn (W. Chen).

http://dx.doi.org/10.1016/j.jallcom.2015.04.072
0925-8388/

for the synthesis of silver based delafossite oxides are much fewer. The inherent cause is suggested to derive from the fact that, the simple binary oxide of silver (Ag_2O) is easy to decompose at a temperature of ~300 °C, which limits the preparation of silver based delafossites through solid-state reactions. Therefore, it becomes a reasonable choice to synthesize silver based delafossite oxides at low-temperature and/or closed reaction systems [2,27]. For example, $AgCrO_2$ crystals with an average size of around 1 μm have been synthesized through cation exchange reactions, by heating $LiCrO_2$, KNO_3 and $AgNO_3$ at 350 °C in an evacuated silica tube for 4 days [19,21]. Recently, $AgCrO_2$ crystals with an average size of 2 μm have been prepared under a critical hydrothermal condition (400 °C, 40 MPa) [27]. Note that, those reported processes are complicated and include tough conditions; to synthesize nano-sized silver based delafossite oxides still remains as great challenge.

In this work, delafossite $AgCrO_2$ nanocrystals with ultrafine sizes of 10–20 nm have been synthesized for the first time via a low temperature hydrothermal method, and its potential as photocathode in p-type DSSC has been primarily examined. The synthesis parameters effecting on the crystal phases and morphologies have been studied. The element composition and valence state information, thermal stability, electrical and optical properties of $AgCrO_2$ nanocrystals have been systematically investigated. At last, a general crystal formation mechanism for the hydrothermal synthesis of chromium based delafossite oxides ($AgCrO_2$ and $CuCrO_2$ nanocrystals) based on the in-situ oxidation–reduction reactions have been proposed.

2. Experimental section

All of the chemicals in these experiments without special notification were purchased from Sigma Aldrich with analytical grade and used without further purification. In a typical hydrothermal synthesis, certain amounts of reactants were dissolved in deionized water, and the obtained solution was transferred into a Teflon-lined autoclave. The sealed autoclave was maintained at 190–230 °C for reaction. After the reaction finished, the autoclaves were naturally cooled to room temperature. Finally, the obtained precipitate was washed for several times in a centrifugal cleaning machine and was finally stored in absolute alcohol solution for further use.

Powder X-ray diffraction patterns were collected at room temperature by using a Panalytical X'pert Pro diffractometer (XRD, Cu Kα radiation). A field emission scanning electron microscope (FESEM) system (Hitachi-S-4800) coupled with energy dispersive X-ray spectroscopy (EDX) and a transmission electron microscope (FETEM, Tecnai G2 F30) were used to observe the microstructure and determine the composition of the as-synthesized nanocrystals. The thermal stability of nanocrystals was investigated by a differential scanning calorimeters-thermo gravimetric analyzer (DSC-TG, Diamond TG/DTA, Perkin–Elmer Instruments), these samples were heated in air from room temperature to 800 or 1000 °C at a heating rate of 10 °C min^{-1}. The ultraviolet–visible–near infrared (UV–vis–NIR) spectra of films were recorded on a Perkin–Elmer UV/Vis spectrophotometer (UV–vis, Model Lambda 950) in the wavelength range of 300–800 nm. Hall effect measurements were done on a Hall effect analysis system (Accent HL 5500 PC), of which the samples were prepared by the powder pellet method, using Ag coating at four contact points to decrease the contact resistance. X-ray photoelectron spectroscopy measurements (XPS) were performed with a physical electronics surface analysis equipment (Model PHI 5600), and the C (1s) line (at 285.0 eV) corresponding to the surface adventitious carbon (C–C line bond) has been used as the reference binding energy. By using a mask with a size of 4.5 × 4.5 mm^2 to prevent the scattering of light, the solar cells were tested using a solar simulator with an AM 1.5 G filter (Oriel, model 91192) at a light intensity of 100 mW cm^{-2}, and calibrated using a standard silicon reference cell.

3. Results and discussion

3.1. Hydrothermal synthesis of $AgCrO_2$ nanocrystals

$AgCrO_2$ nanocrystals were prepared similarly to our previously hydrothermal procedure for $CuCr_{1-x}Mg_xO_2$ ($x = 0$, 0.05, 0.10.) [11,12]. At first, 15 mMol $Cr(NO_3)_3{\cdot}9H_2O$ and 15 mMol $AgNO_3$ were dissolved in 70 ml deionized water at room temperature, 2.40 g NaOH was added to the above solution and stirred for 10 min. After reaching a homogeneous state, the solution was loaded into a 100 ml Teflon-lined autoclave, which was sealed and maintained at 190–230 °C for 60 h. After the reaction finished, the obtained yellow green precipitate was washed with diluted nitric acid, deionized water and absolute alcohol in sequence for several times, and then stored in absolute alcohol solution. Finally, about 2.0 g nano-sized $AgCrO_2$ product could be gained from each reaction.

Fig. 1 shows the XRD patterns and morphologies of $AgCrO_2$ nanocrystals prepared at different reaction temperature (190 °C, 210 °C and 230 °C). Fig. 1a shows that all of the diffraction peaks can be indexed to delafossite $AgCrO_2$ (JCPDS File Card No. 70-1703) with the hexagonal R3m crystal structure, and no impurity phase can be detected. The full width at half maximum of the XRD patterns becomes wider as the reaction temperature decreases, which reflects the crystal size decreases. By applying the Scherrer equation to the broadened diffraction peaks, the average crystal sizes at different synthesis temperatures of 190 °C, 210 °C and 230 °C were calculated to be 18.4 nm, 15.9 nm and 14.1 nm, respectively. This result is consistent with their corresponding SEM and TEM images in Fig. 1b–d. From TEM images, the nanocrystals are with the hexagonal nanoplates morphology. The observed diameters of the nanoplates obtained at 230 °C, 210 °C and 190 °C are 15–50 nm, 15–30 nm and 10–30 nm, respectively, while their thicknesses are much thinner. From these, it is known that the decreased reaction temperature leads to slower crystal growth rate, and therefore smaller crystal size of the nano-products.

Furthermore, the SEM–EDS mapping results of $AgCrO_2$ nanocrystals are shown in Fig. 2, to reduce the measurement errors caused by absorption of water molecules on the sample surface, the $AgCrO_2$ was analyzed after annealing at 120 °C for 2 h in vacuum. It can be observed that all of the Ag, Cr and O elements are homogeneously distributed (Fig. 2a–c), the elementary percentages of Ag (25.75 at.%), Cr (26.88 at.%), O (47.37 at.%) are nearly consistent with their source materials' concentrations in the hydrothermal precursor and close to the stoichiometric proportion of $AgCrO_2$ (Ag: Cr: O = 1: 1.04: 1.84, see Fig. 2e). In addition, the elemental chemical states of the $AgCrO_2$ crystals have been investigated by XPS. The corresponding results are shown in Fig. 3. The peaks located at near 368.5 eV (Ag 3d 5/2) and 373.9 eV (Ag 3d 3/2) shown in Fig. 3a confirm the monovalent state of silver element (Ag^+) in the samples [20]. The peaks located at near 576.3 eV and 585.8 eV (Fig. 3b) are corresponding to the binding energies of Cr 2p 3/2 and Cr 2p 1/2, which confirm the trivalent state of chromium element (Cr^{3+}) in the samples [12,26].

3.2. Thermal stability of $AgCrO_2$ nanocrystals

From the thermogravimetric (TG) curve shown in Fig. 4a, the initial weight losses of $AgCrO_2$ samples are suggested to be due to the evaporation of chemically combined water of crystallization and the variation of oxygen vacancy in the sample. The sharp mass decrease from the temperature of above 400 °C should be due to $AgCrO_2$ decomposition in air at the temperature. Fig. 4b shows the diffraction patterns of $AgCrO_2$ samples sintered in air at 350 °C, 400 °C, 500 °C, and 550 °C for 1 h, respectively. The diffraction peaks of the $AgCrO_2$ powder sintered at 350 °C should be identified as pure $AgCrO_2$ crystal phase; whilst for the $AgCrO_2$ powder sintered at 550 °C, the diffraction peaks owning to the newly generated by-products of Ag (JCPDS File Card No. 65-8428) and Cr_2O_3 (*, JCPDS File Card No. 38-1479) could be clearly identified. The appearance of Cr_2O_3 inside the $AgCrO_2$ powders sintered at the temperatures of >400 °C suggests that the decomposition of $AgCrO_2$ occurs. This phenomenon is consistent well with the TG analysis result. It is suggested that the following chemical reaction

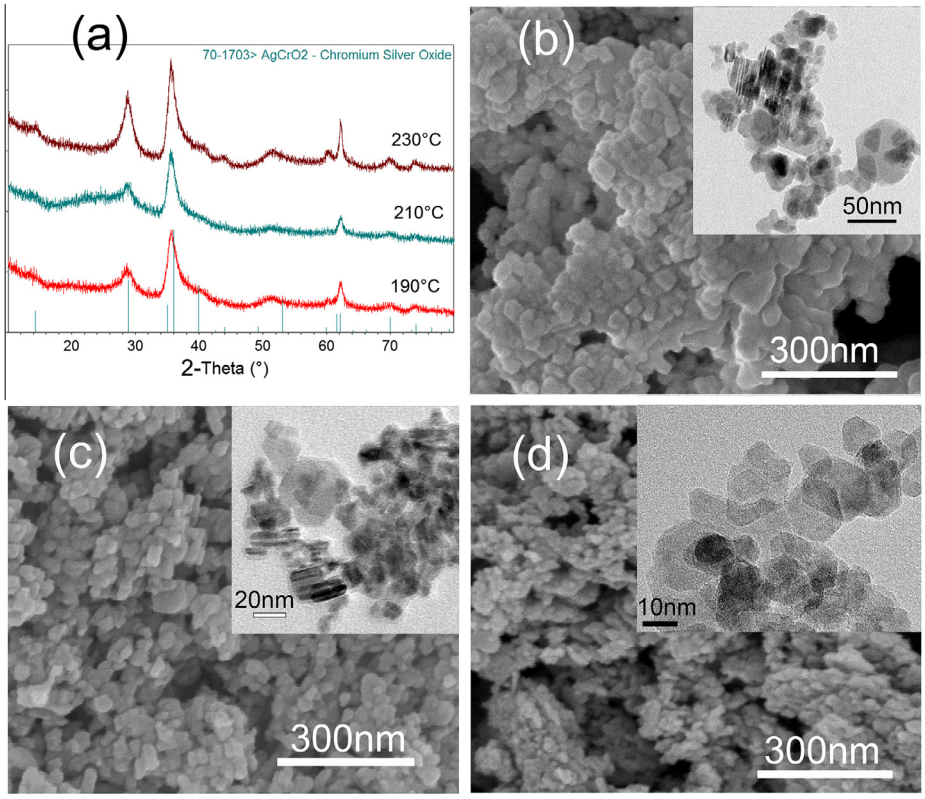

Fig. 1. XRD patterns (a) of products freshly obtained $AgCrO_2$ nanocrystals from the hydrothermal synthesis at 190–230 °C. Also shown are SEM and TEM images of freshly obtained $AgCrO_2$ nanocrystals (b, 230 °C; c, 210 °C; d, 190 °C).

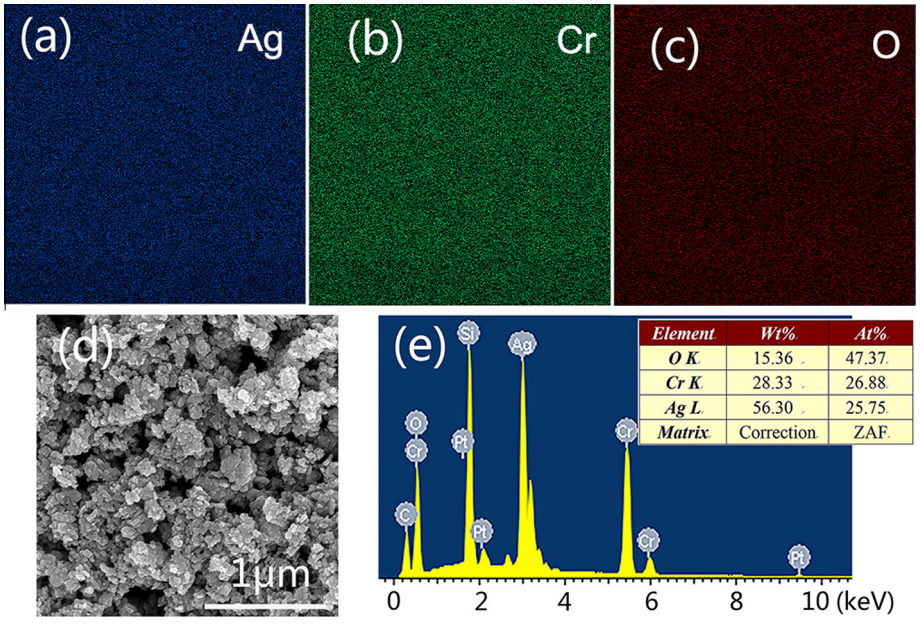

Fig. 2. (a–c) EDS elemental mapping, (d) SEM image, and (e) elemental analysis report of the $AgCrO_2$ nanocrystals.

should be involved during the high temperature (>400 °C) sintering:

$$4AgCrO_2 = 2Cr_2O_3 + 4Ag + O_2 \quad (1)$$

On the contrary, according to our previous work [11], the TG curve of $CuCrO_2$ shows that mass increases sharply from the temperature of above 450 °C, which should be due to the oxidation of $CuCrO_2$ [11]. The above mentioned thermal stability of $CuCrO_2$/$AgCrO_2$ are similar to our previous report on thermal stability of $CuAlO_2$/$AgAlO_2$ [3]. It is common that Cu based delafossite oxides tend to be oxidized by O_2 in the air at higher sintering temperature, whilst Ag based delafossite oxides tend to decompose to be metallic Ag at higher sintering temperature. If one compares the thermal stability of Al based delafossite oxides and Cr based delafossite

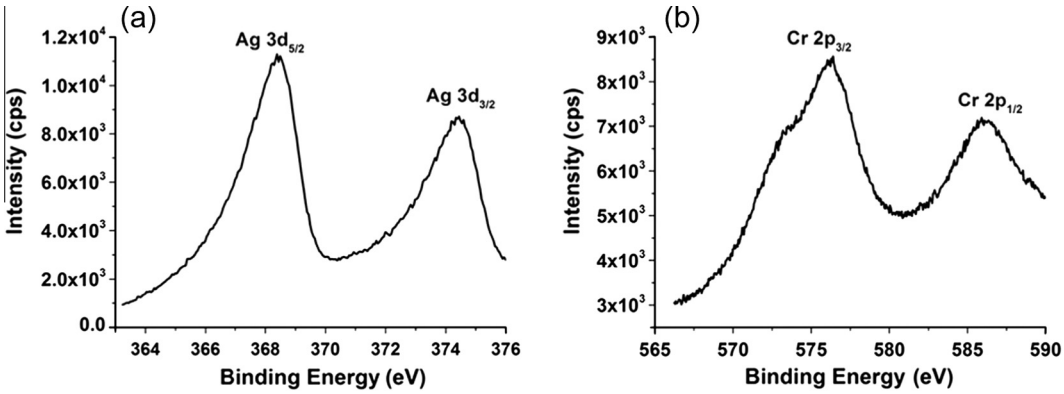

Fig. 3. Typical XPS spectra of $AgCrO_2$ nanocrystals: (a) Ag 3d and (b) Cr 2p.

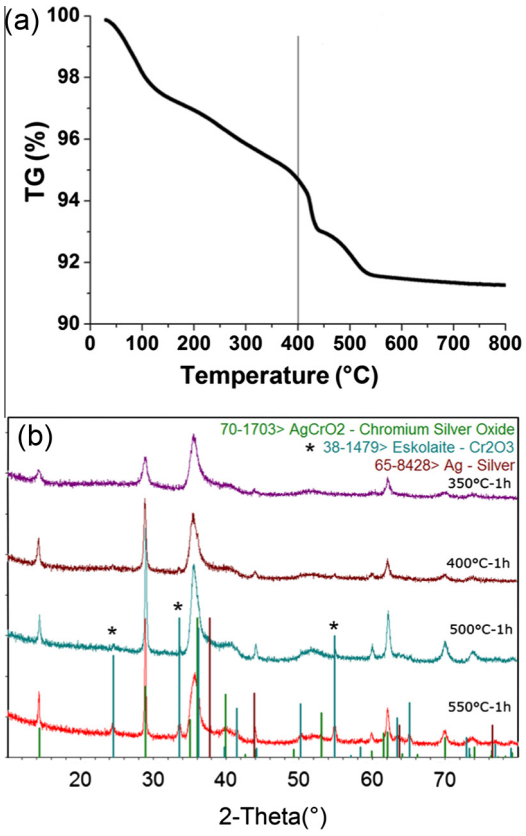

Fig. 4. Thermogravimetric (TG) curves of (a) $AgCrO_2$ at a heating rate of 10 °C min^{-1} in air. Also shown are the corresponding XRD patterns for (b) $AgCrO_2$ powder after sintering in air at different temperatures.

oxdies, the former samples are with much higher decomposition temperature of ~800 °C, about 400 °C higher than that of the latter ones. From these, it can be deduced that the thermal stability of the AMO_2s are closely related to the M site elements. Since AlO_6 octahedras are more stable and with stronger interaction toward A site Cu^+ or Ag^+ than CrO_6 octahedras, therefore Al based delafossite oxides with better phase stability than that of Cr based delafossite oxides are understandable.

3.3. Hall effect measurements on $AgCrO_2$ nanocrystals

The Hall Effect measurement results of $AgCrO_2$ and $CuCrO_2$ delafossite oxides are shown in Table 1. All these delafossite oxides were confirmed with p-type conductivity. The conductivity of the delafossite oxides are closely to that of NiO [27], but the carrier densities of Cu based delafossite oxides are several orders of magnitude higher. Moreover, the conductivity and carrier density of $AgCrO_2$ are 2.22×10^{-6} S cm^{-1} and 4.33×10^{11} cm^{-3}, respectively, which are much lower than that of $CuCrO_2$. This low conductivity problem of $AgCrO_2$ is consistent with Poeppelmeier's report [30]. They demonstrated that the conductivities of silver delafossites are much lower than that of copper delafossites with the same M-site cations, and suggested that the mixed valence state from O-2p and Ag-4d limits the hole mobility, resulting in the low conductivity of silver delafossites [19,30].

3.4. Optical properties of $AgCrO_2$ nanocrystals

In order to study the optical properties of p-type $AgCrO_2$ nanocrystals, uniformity films were deposited on the glass slides through spray deposition method. After heated in air at 300 °C for 1 h, the deposited films were examined by the UV–Vis spectroscopy. The optical bandgaps are estimated by the following equation: [3,31,32]

$$(\alpha h\upsilon)^{1/n} = A(h\upsilon - E_g) \quad (2)$$

where α, h, υ, A, and E_g are the absorption coefficient, Planck constant, the frequency of light, a constant, and the band gap, respectively. Moreover, the exponent n depends on the type of transition, for direct-allowed transition, $n = 1/2$; for indirect-allowed transition, $n = 2$, for direct-forbidden transition, $n = 3/2$, and for direct-forbidden transition, $n = 3$ [3].

Fig. 5 shows the optical transmittance spectra within the wavelength range of 300–800 nm and the calculated bandgaps of $AgCrO_2$ films. In detail, the average optical transmittance of greenish-yellow $AgCrO_2$ film (about 2.0 μm) is around 60–75% in visible range (Fig. 5a), and the direct bandgap of $AgCrO_2$ is around 3.32 eV (Fig. 5b). The calculated bandgap value of $AgCrO_2$ is much bigger than that of $CuCrO_2$ (3.25 eV) [32], this phenomena is similar to our previous report on that of $CuAlO_2/AgAlO_2$ [3]. And the larger optical bandgap of $AgCrO_2$ is suggested to be owing to the shift

Table 1
The test results of Hall Effect measurements for $CuCrO_2$ and $AgCrO_2$ Nanocrystals.

Materials	Type	Conductivity (S cm^{-1})	Carrier density (cm^{-3})	Hall coefficient (cm/C)
NiO [24]	p	8.33E−05	3.91E+11	–
$CuCrO_2$	p	4.60E−05	4.86E+13	1.29E+05
$AgCrO_2$	p	2.22E−06	4.33E+11	1.44E+01

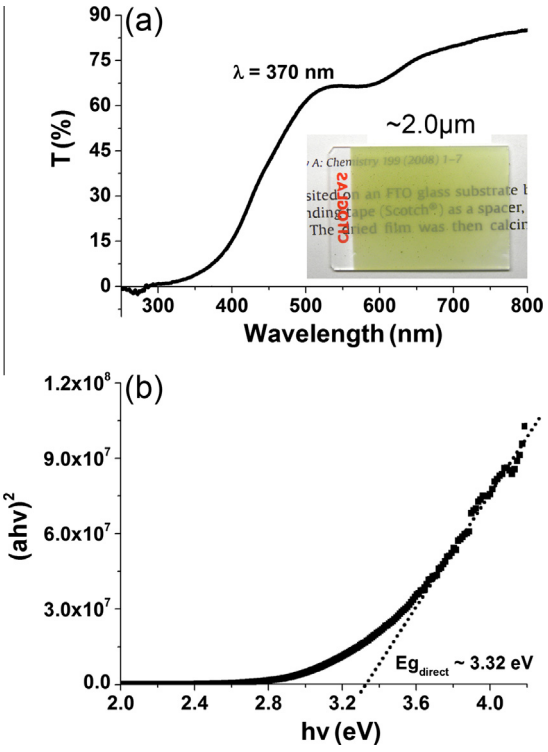

Fig. 5. The optical transmittance (a) and the calculated bandgap (b) of $AgCrO_2$ films; the inset in (a) is corresponding optical image.

of valence band states toward to lower energy, associated with the replacement of copper 3d states with silver 4d states [3,30].

3.5. The proposed synthesis mechanisms for $AgCrO_2$

High temperature solid-state reaction and hydrothermal reaction are the most common methods used for preparing the copper based delafossite oxides (such as $CuAlO_2$, $CuCrO_2$ and $CuFeO_2$) [30,34]. However, until now, there has been very few literatures except the following ones focusing on the hydrothermal synthesis mechanisms [3,26,27]. For example, Kenneth R. Poeppelmeier and coworkers reported the synthesis of broad families of delafossite oxides for $CuMO_2$ (M = Al, Sc, Cr, Mn, Fe, Co, Ga, and Rh), and $AgMO_2$ (M = Al, Sc, Fe, Co, Ni, Ga, Rh, In, and Tl) [2]. Unfortunately, their report did not involve $AgCrO_2$. Xiaodong Fang and coworkers reported the hydrothermal synthesis of $CuCrO_2$ at 220 °C by using Cu_2O, $Cr(NO_3)_3$ and NaOH as the reactants [26]. They demonstrated that aqueous soluble $Cu(OH)^{2-}$ and $Cr(OH)^{4-}$ species result in eruptible nucleation of $CuCrO_2$. W. C. Sheets and coworkers have tried the hydrothermal synthesis of $AgCrO_2$ at 210 °C by using Ag_2O and $Cr(OH)_3$ dissolved in 2.5 M NaOH solution, but no $AgCrO_2$ crystal has been obtained; only silver metal and highly soluble CrO_4^{2-} species were stabilized [2]. Recently, Sanjay Kumar and coworkers reported that $AgCrO_2$ polycrystalline (with average size about 2 μm, much bigger than our $AgCrO_2$ nanocrystals) were synthesized by one-step reaction between Ag_2O and $Cr(OH)_3$ in supercritical water conditions (400 °C, 40 MPa), using $K_2Cr_2O_7$ as an oxidizing agent through hydrothermal method [27]. Just like the statements from Xiaodong Fang, Sanjay Kumar also declared that only at a certain temperature, pressure, reaction time and $K_2Cr_2O_7$ as the oxidizing agent, the stability of $Ag(OH)^{2-}$ and $Cr(OH)^{4-}$ species could be guaranteed, and finally the supersaturation state was reached and then $AgCrO_2$ was obtained.

In this work, during the hydrothermal synthesis of $AgCrO_2$, the original reaction products include Ag, $AgCrO_2$, Na_2CrO_4 and $NaNO_3$ from the XRD patterns in Fig. 6a. It is suggested that part of silver cations (Ag^+) were reduced to elemental silver (Ag), accompanied with part of trivalent chromium cations (Cr^{3+}) were oxidized to hexavalent chromium cations (Cr^{6+}). Finally, we can get the pure phase $AgCrO_2$ nanocrystals after the corresponding washing procedure, by which the other byproducts were dissolved and washed off as ions. Moreover, the similar circumstance was present in the preparation of $CuCrO_2$ [11,12]. From the XRD patterns of Fig. 6b, it can be seen that CuO, $CuCrO_2$, Na_2CrO_4 and $NaNO_3$ were detected in the origin reaction products for $CuCrO_2$; it is suggested that cupric cations (Cu^{2+}) were reduced to cuprous cations (Cu^+), accompanied with part of trivalent chromium cations (Cr^{3+}) were oxidized to hexavalent chromium cations (Cr^{6+}). After these reaction products were washed with diluted hydrochloric acid and absolute alcohol, pure phase $CuCrO_2$ nanocrystals could be obtained.

In summary, we prepared both $AgCrO_2$ and $CuCrO_2$ nanocrystals similarly from metal nitrates ($Cu(NO_3)_2$ or $AgNO_3$ and $Cr(NO_3)_3$) and sodium hydroxide (NaOH) [11,12]. It can be concluded that the in-situ oxidation–reduction reactions during the hydrothermal process play the critical role for the crystal formation of desired delafossite oxides. The chemical reactions can be written as the following equations:

$$3Ag^+ + Cr^{3+} = 3Ag + Cr^{6+} \quad (2\text{-a})$$

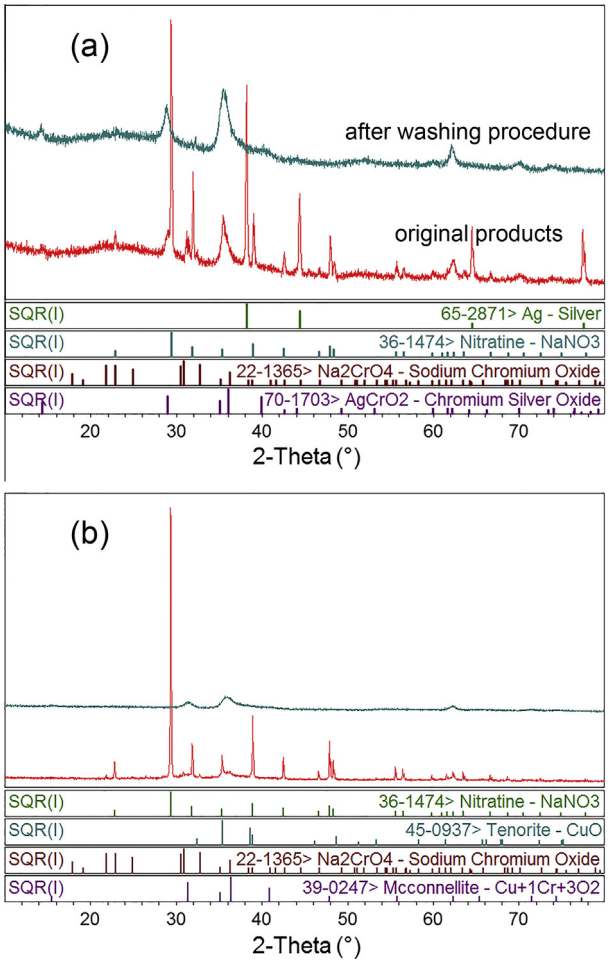

Fig. 6. XRD patterns of reaction products for the preparation of (a) $AgCrO_2$ and (b) $CuCrO_2$.

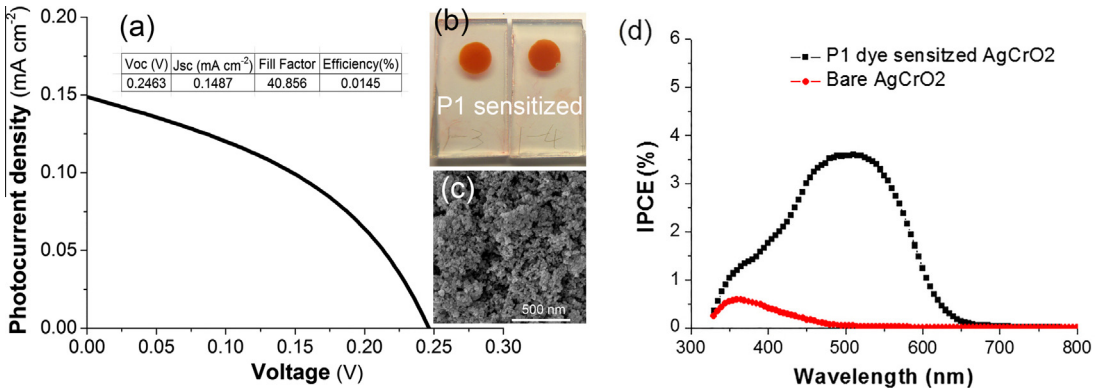

Fig. 7. (a) *J–V* characteristic curve based on $AgCrO_2$ photocathode, (b) digital photo of P1 dye sensitized $AgCrO_2$ photocathode, (c) SEM image of mesoporous $AgCrO_2$ film and (d) IPCE spectra of the solar cells based on bare $AgCrO_2$ and P1 dye sensitized $AgCrO_2$ photocathode.

$$Ag^{+} + Cr^{3+} + 4OH^{-} = AgCrO_2 + 2H_2O \quad (2\text{-b})$$

$$3Cu^{2+} + Cr^{3+} = 3Cu^{+} + Cr^{6+} \quad (2\text{-c})$$

$$Cu^{+} + Cr^{3+} + 4OH^{-} = CuCrO_2 + 2H_2O \quad (2\text{-d})$$

As mentioned above, the synthesis mechanism of chromium based delafossite oxides ($AgCrO_2$ and $CuCrO_2$ nanocrystals) based on an oxidation–reduction reaction was pointed out for the first time. This novel synthesis mechanism based on an oxidation–reduction reaction between the A site and M site elements in AMO_2, which is totally different from the combination reaction taking place during the high-temperature solid-state method. On the basis of this mechanism, we may propose a novel and general approach for the preparation of large families of delafossite oxides, especially for the M-site element of AMO_2 can change their valence states during the hydrothermal conditions.

3.6. Application in dye-sensitized solar cells

In our previous reports [11,12], both $CuCrO_2$ (~15 nm) and $CuCr_{0.90}Mg_{0.10}O_2$ (~10 nm) nanocrystals were successfully employed to fabricate photocathodes for p-type DSSCs. In this work, we first applied $AgCrO_2$ nanocrystals as photocathodes in p-type DSSCs, using P1 dye as the sensitizer. The detailed solar cell fabrication and measurement are according to our previous works [11,12]. Fig. 7a presents the photocurrent–voltage (*J–V*) curve of the P1 dye sensitized $AgCrO_2$ based p-type DSSC under 1 Sun AM 1.5G illumination. An open-circuit voltage (V_{oc}) of 246 mV, short-circuit current density (J_{sc}) of 0.149 mA cm^{-2}, fill factor of 0.409, and overall photoconversion efficiency of 0.0145% could be achieved. From Fig. 7b, the P1 dye sensitized $AgCrO_2$ film presents cardinal red color, which proves abundant P1 dye molecules absorbing on the mesoporous film. Moreover, the highly porous morphology of $AgCrO_2$ film shown in Fig. 7c can explain its good dye absorbing capability. Though, the V_{oc} of $AgCrO_2$ based p-type DSSC is very high in comparison to most of previously reported p-type DSSCs based on P1 dye, the J_{sc} is very low, only 0.149 mA cm^{-2}. These result in the DSSC device with an inefficient efficiency of around 0.0145%. The low IPCE shown in Fig. 7d can explain the very low J_{sc} of the solar cell. The IPCE spectral difference before and after P1 dye sensitization on the $AgCrO_2$ photocathodes can prove the presence of the sensitization effect in the p-type DSSC. It is known that IPCE of p-type DSSC is determined by synergistic effect of (1) light harvesting of dye sensitized photocathode, (2) hole injection from P1 dye to valance band of $AgCrO_2$ and (3) the hole collection through the $AgCrO_2$ network. Which effect plays the decisive role on the poor device performance needs to be further elucidated and resolved in the following work. At the moment, the low conductivity of $AgCrO_2$ and/or improper band alignment between P1 dye and $AgCrO_2$ should be firstly suspected.

4. Conclusions

In summary, we report a novel, controllable and one-step synthesis of p-type delafossite oxides $AgCrO_2$ nanocrystals by a low-temperature (190–230 °C) hydrothermal method and, the $AgCrO_2$ nanocrystals as photocathode material in p-type DSSC for the first time. The obtained nano-sized $AgCrO_2$ crystals are around 10–20 nm, with p-type conductivity, wide bandgap (>3.10 eV) and high optical transparency (60–75%). The synthesis temperatures for $AgCrO_2$ nanocrystals has been expanded to as low as 190 °C, which is much lower than ever reported. According to the analysis of reaction products generated during the hydrothermal process, we have proposed the general synthesis mechanism for these chromium based delafossites ($AgCrO_2$ and $CuCrO_2$ nanocrystals). Only metal nitrates ($AgNO_3$ or $Cu(NO_3)_2$ and $Cr(NO_3)_3$) and sodium hydroxide (NaOH) were selected as starting materials, and therefore formed $CuCrO_2$ and $AgCrO_2$ through an in-situ oxidation–reduction reaction. Namely, the oxidation–reduction reactions occurred between Cr^{3+} and Ag^{+}/Cu^{2+} under facile hydrothermal conditions, and then formed these chromium based delafossites. The proposed synthesis mechanism for this low-temperature hydrothermal method is different from that in traditional high-temperature solid-state method, and our finding may open a new avenue for the preparation of nanocrystals with delafossite structure.

Acknowledgements

The authors would like to express sincere thanks for the financial support by the National Natural Science Foundation of China (Nos. 21103058, 51402223), 973 Program of China (No. 2011CBA00703) and Basic Scientific Research Funds for Central Colleges (HUST: 2012YQ027, 2013TS040). D. Xiong also thanks the financially supported by China Postdoctoral Science Foundation (No. 2014M552098) and the Fundamental Research Funds for the Central Universities (WUT: 2014-IV-091). We also thank Analytical and Testing Center of Huazhong University Science & Technology for the sample measurements.

References

[1] A. Pabst, Am. Mineral. 31 (1946) 539–546.
[2] W.C. Sheets, E. Mugnier, A. Barnabe, T.J. Marks, K.R. Poeppelmeier, Chem. Mater. 18 (2006) 7–20.

[3] D. Xiong, X. Zeng, W. Zhang, H. Wang, X. Zhao, W. Chen, Y.B. Cheng, Inorg. Chem. 53 (2014) 4106–4116.
[4] H. Kawazoe, M. Yasukawa, H. Hyodo, M. Kurita, H. Yanagi, H. Hosono, Nature 389 (1997) 939–942.
[5] J. Ahmed, C.K. Blakely, J. Prakash, S.R. Bruno, M. Yu, Y. Wu, V.V. Poltavets, J. Alloys Comp. 591 (2014) 275–279.
[6] A. Nattestad, X. Zhang, U. Bach, Y.-B. Cheng, J. Photoics. Energ. 1 (2011) 011103.
[7] A. Renaud, B. Chavillon, L. Le Pleux, Y. Pellegrin, E. Blart, M. Boujtita, T. Pauporté, L. Cario, S. Jobic, F. Odobel, J. Mater. Chem. 22 (2012) 14353–14356.
[8] M.Z. Yu, G. Natu, Z.Q. Ji, Y.Y. Wu, J. Phys. Chem. Lett. 3 (2012) 1074–1078.
[9] M. Yu, T.I. Draskovic, Y. Wu, Inorg. Chem. 53 (11) (2014) 5845–5851.
[10] Z. Xu, D. Xiong, H. Wang, W. Zhang, X. Zeng, L. Ming, W. Chen, X. Xu, J. Cui, M. Wang, S. Powar, U. Bach, Y.-B.J. Cheng, Mater. Chem. A 2 (2014) 2968–2976.
[11] D.H. Xiong, Z. Xu, X.W. Zeng, W.J. Zhang, W. Chen, X.B. Xu, M.K. Wang, Y.-B. Cheng, J. Mater. Chem. 22 (2012) 24760–24768.
[12] D.H. Xiong, W.J. Zhang, X.W. Zeng, Z. Xu, W. Chen, M.K. Wang, L.C. Sun, Y.B. Cheng, ChemSusChem 6 (2013) 1432–1437.
[13] X. Xu, B. Zhang, J. Cui, D. Xiong, Y. Shen, W. Chen, L. Sun, Y. Cheng, M. Wang, Nanoscale 5 (2013) 7963–7969.
[14] X. Xu, J. Cui, J. Han, J. Zhang, Y. Zhang, L. Luan, G. Alemu, Z. Wang, Y. Shen, D. Xiong, W. Chen, Z. Wei, S. Yang, B. Hu, Y. Cheng, M. Wang, Sci. Rep. (2014) 4.
[15] F. Odobel, Y. Pellegrin, J. Phys. Chem. Lett. 4 (2013) 2551–2564.
[16] M. Yu, T.I. Draskovic, Y. Wu, Phys. Chem. Chem. Phys. 16 (2014) 5026–5033.
[17] B.J. Ingram, G.B. González, T.O. Mason, D.Y. Shahriari, A. Barnabe, D. Ko, K.R. Poeppelmeier, Chem. Mater. 16 (2004) 5616–5622.
[18] E. Mugnier, A. Barnabé, P. Tailhades, Solid State Ionics 177 (2006) 607–612.
[19] R. Nagarajan, N. Duan, M.K. Jayaraj, J. Lia, K.A. Vanaja, A. Yokochi, A. Draeseke, J. Tate, A.W. Sleight, Int. J. Inorg. Mater. 3 (2001) 265–270.
[20] S. Ouyang, Z. Li, Z. Ouyang, T. Yu, J. Ye, Z. Zou, J. Phys. Chem. C 112 (2008) 3134–3141.
[21] S. Ouyang, N. Kikugawa, D. Chen, Z. Zou, J. Ye, J. Phys. Chem. C 113 (2009) 1560–1566.
[22] M. Shimode, Y. Hayashi, M. Sasaki, K. Mukaida, Mater. Trans. 41 (2000) 1111–1113.
[23] Th. Dittrich, L. Dloczik, T. Guminskaya, M.Ch. Lux-Steiner, N. Grigorieva, I. Urban, Appl. Phys. Lett. 85 (2004) 742.
[24] S. Gao, Y. Zhao, P. Gou, N. Chen, Y. Xie, Nanotechnology 14 (2003) 538.
[25] R. Srinivasan, B. Chavillon, C. Doussier-Brochard, L. Cario, M. Paris, E. Gautron, P. Deniard, S. Jobic, J. Mater. Chem. 18 (2008) 5647–5653.
[26] S. Zhou, X. Fang, Z. Deng, D. Li, W. Dong, R. Tao, G. Meng, T. Wang, X. Zhu, J. Cryst. Growth 310 (2008) 5375–5379.
[27] S. Kumar, M. Miclau, C. Martin, Chem. Mater. 25 (2013) 2083–2088.
[30] W.C. Sheets, E.S. Stampler, M.I. Bertoni, M. Sasaki, T.J. Marks, T.O. Mason, K.R. Poeppelmeier, Inorg. Chem. 47 (7) (2008) 2696–2705.
[31] R. Nagarajan, A.D. Draeseke, A.W. Sleight, J. Tate, J. Appl. Phys. 89 (2001) 8022–8025.
[32] Y.F. Wang, Y.J. Gu, T. Wang, W.Z. Shi, J. Sol–Gel Sci. Technol. 59 (2011) 222–227.
[34] A.P. Amrute, Z. Łodziana, C. Mondelli, F. Krumeich, J. Pérez Ramírez, Chem. Mater. 25 (2013) 4423–4435.